Time and stress history dependency of creep strain vector for granular materials

Le temps et la dependance de la contrainte histoire du fluage deformation pour les granulaire materiel

R.Kuwano – *University of Tokyo, Tokyo, Japan*

ABSTRACT: Creep strains developed in granular materials after three types of loading (isotropic loading ($\Delta\sigma'_h/\Delta\sigma_v'$=1), anisotropic loading ($\Delta\sigma'_h/\Delta\sigma_v'$=0.45) and drained shearing ($\Delta\sigma'_h/\Delta\sigma_v'$=0)) were studied in triaxial tests. Substantial creep strains were observed for each case, which amounted to at least 20% of the instantaneous strains generated during preceding loading, although the amount of creep strains was likely to depend on the loading (rate) conditions. The directions of strain increment vectors during creep were generally similar to those during preceding loading. But in anisotropic loading, strain increment directions during loading and subsequent creep tended to differ. Strain increment vectors showed rotation during creep in drained shearing. It is suggested that the two mechanisms, shear and compression, are acting with different time-dependency, resulting in complicated creep behaviours. Similar implications were also obtained from the change in p' observed during q-constant undrained creep in an undrained triaxial test.

RÉSUMÉ: Le fluage crée dans des matériaux granulaires sous l'influence de trois types de charges affectées de valeur de constante K différentes (charge isotrope ($\Delta\sigma'_h/\Delta\sigma_v'$=1), charge anisotrope ($\Delta\sigma'_h/\Delta\sigma_v'$=0,45) et cisaillèment avec écoulement ($\Delta\sigma'_h/\Delta\sigma_v'$=0)) ont été étudiées par des tests tri-axiaux. Un fluage substantiel a été observe dans chacun des cas, atteignant jusqu'a 20% des contraintes instantanées générées pendant la charge précédente, bienque la proportion de fluage dépendait probablement des conditions d'application de la charge (de son taux). Les directions des vecteurs d'accroissement de la charge étaient généralement similaires a celles utilisées pendant la charge précédente, mais sous pression anisotrope, les directions des contraintes pendant la charge et les directions de fluage tendaient a différér. De plus, les vecteurs d'accroisement des contraintes tournaient pendant le fluage dans le cas du cisaillèment avec écoulement. Nous suggérons que les deux mécanismes de cisailement et de compression agissaient avec des dépendances temporelles différentes avec pour résultat des comportements compliques de fluage. Des conséquences similaires ont aussi été obtenues pour les changements observes de p' pendant le fluage sans cisaillèment aq constant dans un test sous trois axes et sans écoulement.

1 INTRODUCTION

A creep of sand has been usually thought to be small, and sand has been often treated as a practically time-independent material. However, the amount of creep strains of sand in the total strains has been recently noted not to be negligible (e.g. Tatsuoka et al 1998). In this study, the characteristics of creep behaviour are discussed based on the triaxial test results of two granular materials; uniform clean sand and spherical shape glass beads.

2 MATERIALS AND TEST CONDITIONS

Ham River sand (HRS) and Glass Ballotini (GB) were used in this study. HRS is a uniform clean sub-angular medium-fine quartzic sand. GB was spherical in shape and had a similar mean particle size to HRS.

Tiaxial cylindrical specimens (ϕ100mm×h200mm) were fully saturated with an application of 200kPa back pressure, and isotropically or anisotropically consolidated at a rate of $\Delta\sigma_v'$=2kPa/min followed by drained or undrained triaxial compression, during which a number of creep tests were conducted under various stress states.

A load cell was located inside the triaxial cell. The end restraint of the specimen was reduced by means of lubricated ends in order to achieve a uniform deformation as possible. Both axial and radial strains were measured locally at the central height of the specimen. Although the room temperature in the laboratory was controlled within a change of ±Δ1°C (consequently the typical daily variations of cell water temperature were within ±Δ0.5°C), the daily temperature variation was found to cause unacceptable errors to the volume change measurements in the conventional way (measurement of the amount of water that flows in/out of the specimen). Volumetric strains were therefore calculated based on the local axial and radial strains which were less sensitive to the temperature fluctuations. A relatively short term creep behaviour was mainly considered in this study since the creep rates were sufficiently large up to 2~3 hours from the start of creep, compared to the possible measurement errors caused by the sensitiveness of transducers to the temperature variation (Kuwano 1999, Kuwano et al. 2000).

3 DRAINED CREEP DEFORMATION

3.1 *Deformation characteristics during/after isotropic loading*

A dense HRS specimen was isotropically consolidated up to p'=400kPa then swelled back to p'=200kPa. In the course of the isotopic loading/unloading, drained creep tests were carried out

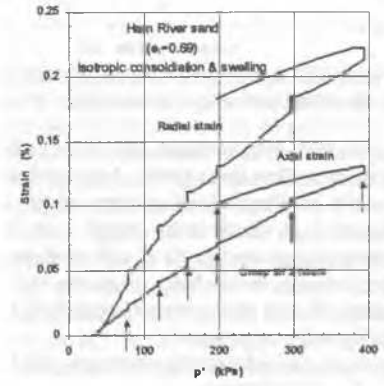

Figure 1. Strain development during isotropic loading/unloading and creep for dense HRS.

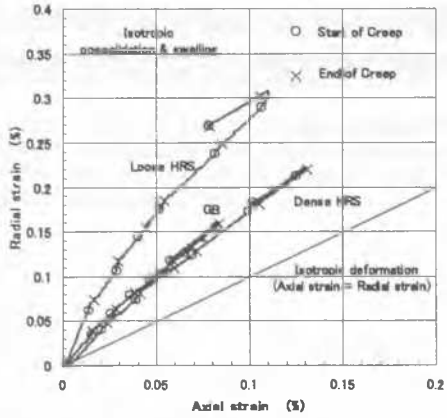

Figure 2. Axial and radial strains for loose/dense HRS and GB samples during isotropic loading/unloading and creep tests.

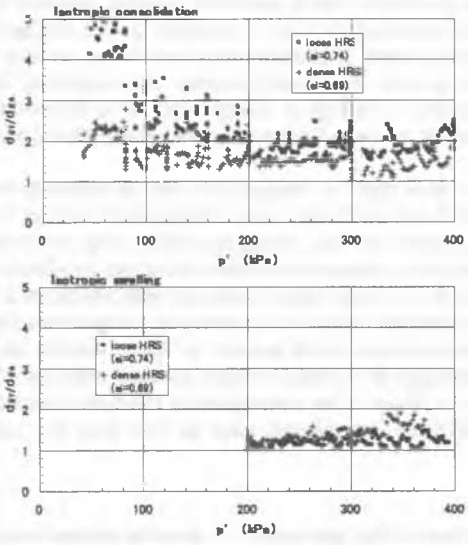

Figure 3. Ratios of radial and axial strain increment for HRS samples during isotropic loading/unloading.

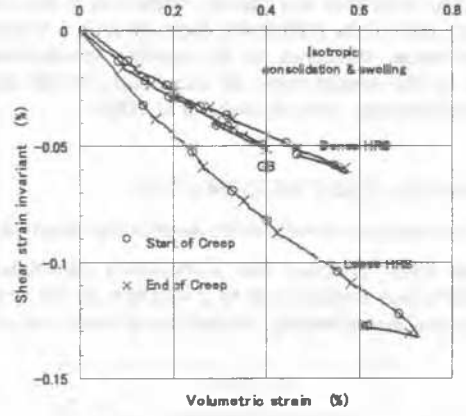

Figure 4. Strain increment directions for loose/dense HRS and GB samples during isotropic loading/unloading and creep tests.

at p'=80, 120, 160, 200, 300, 400 and 200 (after unloading) kPa with a duration of more than three hours. Axial and radial strains developed in whole loading/unloading/creep stages are plotted against p' in Figure 1, in which creep stages were indicated by arrows. Creep strains amounted to 20 to 40% of those developed during preceding loading, while little creep was observed after isotropic unloading. Radial strains were larger than axial strains during both loading and creep stages.

Figure 2 presents the relationship between axial and radial strains developed under isotropic stress states for loose/dense HRS and GB samples. The start and the end of creep stages are indicated by open circle and cross symbols respectively. Anisotropy of the deformation was noticeable in sand as well as glass ballotini. Radial strains were nearly twice as large as axial strains during isotropic stress loading. Radial creep strains were also larger than axial creep strains accordingly. A tendency of softer response in the radial (horizontal) direction was particularly noted for a loose HRS sample at a low pressure range., as shown in Figure 3, in which ratios of radial and axial strain increments, $d\varepsilon_r/d\varepsilon_a$, are plotted against p'. Loose packing appeared to be formed in the horizontal direction at the initial sample setting, as the gravity (in the vertical direction) governed the original stress condition during sample preparation. As the higher isotropic stresses were applied, the pattern of deformation appeared to be changed. At p' levels of more than 200kPa, $d\varepsilon_r/d\varepsilon_a$ values fall in a nearly constant range, around 1.5 to 2.0. On the other hand, the deformation was more isotropic during isotropic unloading with a value of $d\varepsilon_r/d\varepsilon_a \approx 1.3$ for both loose and dense HRS.

Figure 4 presents the pattern of strain development by plotting shear strain invariant, $\varepsilon_s(=2(\varepsilon_a-\varepsilon_r)/3)$, versus volumetric strain. The directions of strain increment for instantaneous strains due to the isotropic loading and those for subsequent creep strains were similar.

3.2 *Deformation characteristics during/after anisotropic loading*

Creep tests were conducted during anisotropic loading on loose/dense HRS and GB. An effective stress path followed and the stress points for creep tests are shown in Figure 5. Specimens were initially consolidated with $\sigma_v'=\sigma_h'=30$kPa (point A), followed the K-constant (=0.45) loading path up to p'=200kPa (point F), then unloaded with Ko swelling path to p'=167kPa. For a GB sample, test was ceased at point F without Ko unloading.

Axial and radial strains for loose HRS developed during entire stages are shown in Figure 6. Creep tests performed in anisotropic loading also showed significant creep strains that reached 30 to 40% of total amount of strains.

Figure 7 shows relationships between axial and radial strains for dense/loose HRS and GB samples under anisotropic stress states. Larger negative radial strains tended to develop during creep and therefore the pattern of strain development appeared to be different between K-constant loading and the subsequent creep period. The directions of the strain increment in terms of

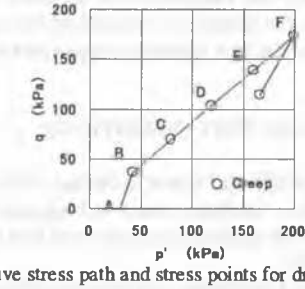

Figure 5. Effective stress path and stress points for drained creep tests.

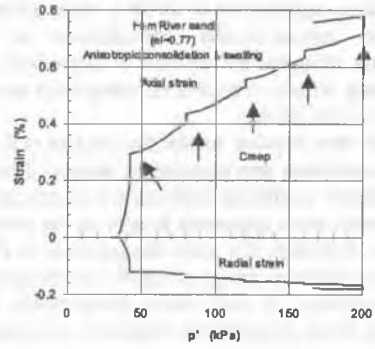

Figure 6. Strain development during anisotropic loading/unloading and creep for loose HRS.

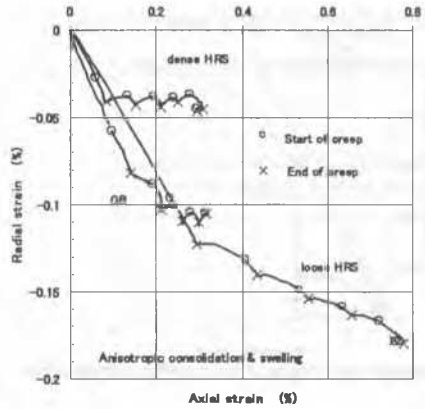

Figure 7. Axial and radial strains for loose/dense HRS and GB samples during anisotropic loading/unloading and creep tests.

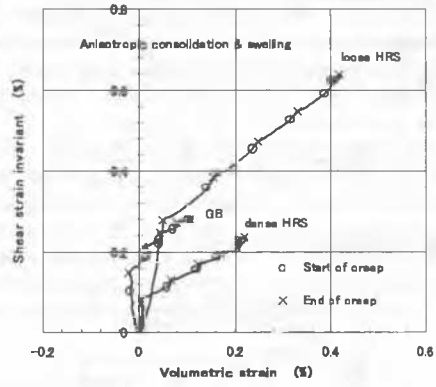

Figure 8. Strain increment directions for loose/dense HRS and GB samples during anisotropic loading/unloading and creep tests.

ε_{vol} and ε_s are given in Figure 8, showing that the strain directions in the creep stages were generally similar to those in the previous loading, but the inclination of strain vectors (ε_{vol}, ε_s) became steeper during a creep period. The fact that $|\varepsilon_s/\varepsilon_{vol}|$ seemed to be larger in creep strains indicated that the volumetric creep might be stabilised earlier than the shear creep.

A stress ratio, $K=\sigma_h'/\sigma_v'$, was 0.45 at the points B to F (in Figure 5) where the creep tests were conducted. The creep strain directions varied when the effective stress increment directions during preceding loading were different. It can be therefore said that the creep behaviour cannot be expressed only by the current stress states, but also by the previous stress or strain history.

3.3 *Creep deformation during/after drained sheairng*

The aforementioned creep behaviour at anisotropic effective stress states was more noticeable when the specimens were subjected to the drained shear. A GB sample was sheared in drained triaxial compression at an axial strain rate of 0.5%/hour, following isotropic consolidation (to p'=400kPa) and swelling (to p'=200kPa). In the course of drained compression, a series of creep tests were performed at the stress points shown in Figure 9. Larger creep deformation occurred at larger shear stress levels, as shown in the stress-strain relationship in Figure 10.

Strain increment direction is given in Figure 11. The creep strains developed in the similar direction to that in the previous loading stage right after the start of creep period although $|\varepsilon_s/\varepsilon_{vol}|$ became slightly larger. However, the rotation of (ε_{vol}, ε_s) vectors occurred soon, then the volumetric strains eventually tended to become positive.

4 UNDRAINED CREEP BEHAVIOUR

Constant q (undrained creep) tests were performed at several shear stress levels during undrained compression on an isotropically consolidated/swelled HRS sample. A typical creep period

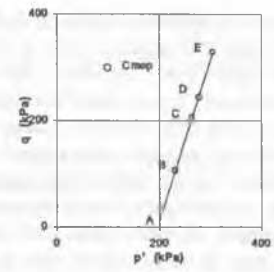

Figure 9. Effective stress path and stress points for drained creep tests.

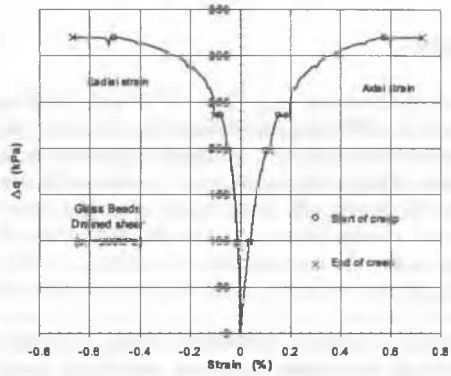

Figure 10. Stress-strain relationship for a drained triaxial compression test on GB.

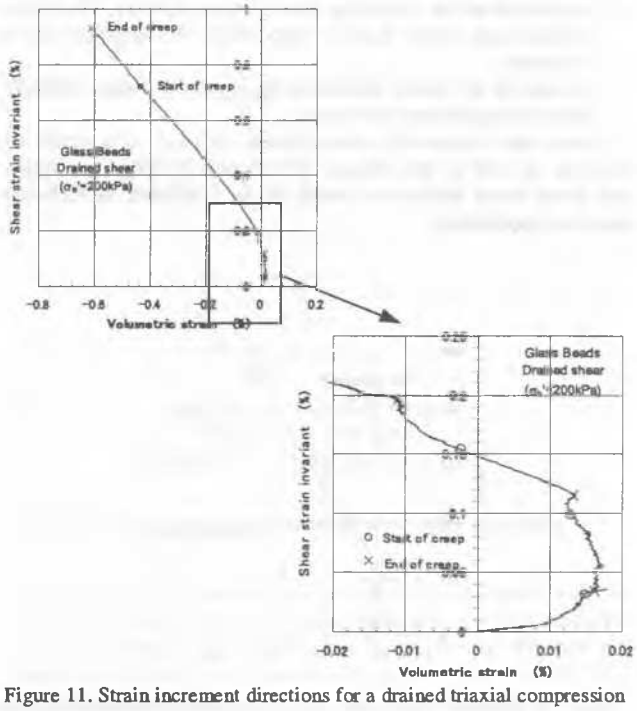

Figure 11. Strain increment directions for a drained triaxial compression test on GB.

was 5 to 10 minutes. An effective stress path and a stress-strain curve are given in Figures 12 and 13 respectively. Figure 14 presents creep strain development with elapsed time, showing that the degree of creep phenomena became more significant as the shear stress levels increased up to the phase transformation point (PTP), after which similar creep rates were seen at different shear stress levels. Figure 15 indicates that the initial undrained creep strain rate has a close relation to the stress ratio, q/p'.

The change of mean effective stress, p', during undrained creep was analogous to the behaviour of volumetric creep strains in the drained shear. Figure 16 shows the variation of p' with time during undrained creep. When the stress-strain behaviour was contractant before the PTP (q=30, 100, 150kPa), the change of p' during undrained creep was negative. At the PTP where the

specimen started to show dilatant behaviour (q=200kPa), the $\Delta p'$ in the creep period was still negative, and at larger shear stress level after the PTP (q=250, 415, 815kPa) , the value of $\Delta p'$ became positive, i.e. dilatant. It was noted that when the undrained creep was continued more than about one hour at q=815kPa, the change of p' turned to be negative and started to show contractant behaviour. Dilatant creep behaviour caused by undrained shearing appeared to be diminished and contractant tendency due to the effective confined pressure seemed to become dominant. Granular materials may become contractant in the stabilization process of creep in the long term.

5 SUMMARY

Experimental observations (e.g. Oda, 1972) and DEM analysis (e.g. Jardine et al, 1999) suggested that, from microscopic point of view, deformation of granular materials appears to be the continuous process of formation/recession of columns that consist of granular particles dominantly in the major principal stress direction. Creep is a stabilisation process of the formation of particles' columns under the constant stress condition. In this study, the following points are noted from the macroscopic observations.

- Deformation anisotropy exhibited during isotropic loading/unloading for tested granular materials, sands and spherical shaped glass ballotini.
- The directions of strain increment vector during creep were dependent on the preceding stress (strain) history. The strain vectors may rotate during creep under the constant stress condition.
- Change in p' during undrained (q-constant) creep similarly showed complicated behaviour.

Shear and volumetric creep strains develop as a result of shearing as well as the change of effective confined pressures, and these creep behaviours seem to be stabilised in different manners respectively.

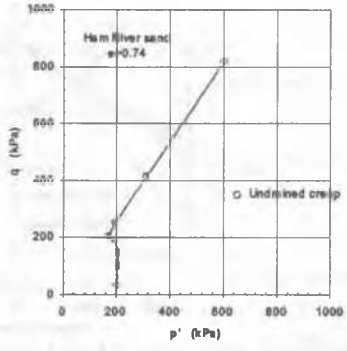

Figure 12. Effective stress path in an undrained compression test on HRS and the stress points of undrained creep tests.

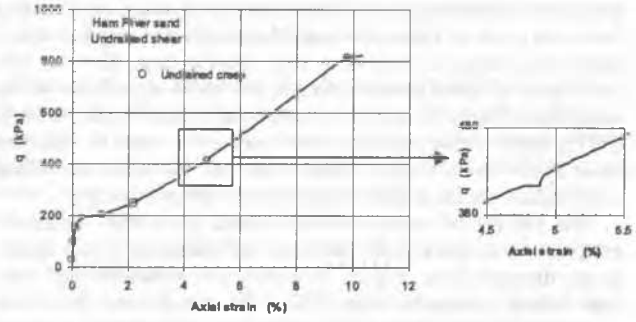

Figure 13. Stress-strain relationship for an undrained triaxial compression test on HRS.

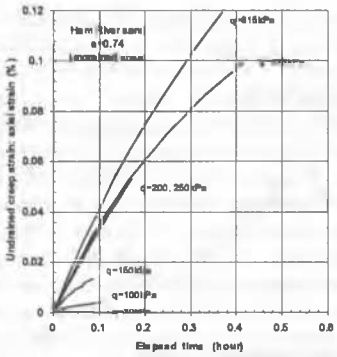

Figure 14. Undrained creep strains at various shear stress levels.

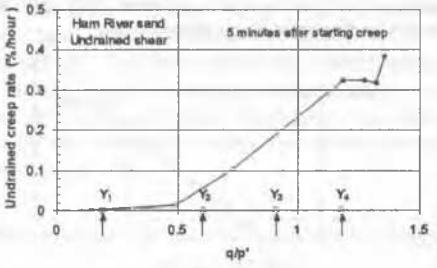

Figure 15. Rates of undrained creep strain.

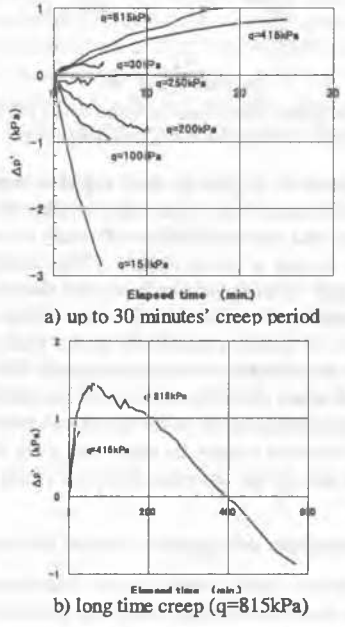

a) up to 30 minutes' creep period

b) long time creep (q=815kPa)

Figure 16. Change in p' during undrained creep.

REFERENCES

Kuwano, R., Connolly, T.M. and Jardine, R.J. 2000. Anisotropic Stiffness Measurements in a Stress-path Triaxial Cell. *Geotechnical Testing Journal*, Vol. 23, No.2,141-157

Kuwano, R. 1999. The stiffness and yielding anisotropy of sand. *Ph.D. Thesis*, Imperial College, University of London

Oda, M. 1972. Initial fabrics and their relations to mechanical properties of granular materials. *Soils and Foundations*, Vol.12, No.1: 17-36,

Jardine, R. J., Kuwano, R., Zadravkovic, L. and Thornton, C. 1999. Some fundamental aspects of the pre-failure behaviour of granular soils. *Key note lecture, 2nd International Symposium on Pre-failure Deformation Characteristics of Geomaterials*, Torino

Tatsuoka,F., Santucci de Magistris,F., Hayano,K., Momoya,Y. and Koseki,J. 1998. Some new aspects of time effects on the stress-strain behaviour of stiff geomaterials. *Keynote Lecture, The Geotechnics of Hard Soils – Soft Rocks, Proc. of Second Int. Conf. on Hard Soils and Soft Rocks*, Napoli (Evamgelista and Picarelli eds.), Balkema, Vol.2